

Contents lists available at ScienceDirect

Science Bulletin

journal homepage: www.elsevier.com/locate/scib



Article

Testing a quantum error-correcting code on various platforms

Qihao Guo ^{a,b,c,1}, Yuan-Yuan Zhao ^{d,c,1}, Markus Grassl ^{e,f}, Xinfang Nie ^{g,h}, Guo-Yong Xiang ^{d,*}, Tao Xin ^{g,h,*}, Zhang-Qi Yin ⁱ, Bei Zeng ^{j,*}

- ^a Institute for Quantum Computing, Baidu Research, Beijing 100193, China
- ^b Department of Applied Physics, Xi'an Jiaotong University, Xi'an 710049, China
- ^c Center for Quantum Computing, Peng Cheng Laboratory, Shenzhen 518055, China
- ^d CAS Key Laboratory of Quantum Information, University of Science and Technology of China, Hefei 230026, China
- ^e Max Planck Institute for the Science of Light, 91058 Erlangen, Germany
- f International Centre for Theory of Quantum Technologies, 80-308 Gdańsk, Poland
- s Shenzhen Institute for Quantum Science and Engineering and Department of Physics, Southern University of Science and Technology, Shenzhen 518055, China
- h Guangdong Provincial Key Laboratory of Quantum Science and Engineering, Southern University of Science and Technology, Shenzhen 518055, China
- i Center for Quantum Technology Research and Key Laboratory of Advanced Optoelectronic Quantum Architecture and Measurements (MOE), School of Physics, Beijing Institute of Technology, Beijing 100081, China
- ^j Department of Physics, The Hong Kong University of Science and Technology, Hong Kong, China

ARTICLE INFO

Article history: Received 18 February 2020 Received in revised form 2 June 2020 Accepted 20 July 2020 Available online 3 August 2020

Keywords:
Quantum error correction
Quantum computation
Superconducting circuit
NMR system
Optical platform

ABSTRACT

Quantum error correction plays an important role in fault-tolerant quantum information processing. It is usually difficult to experimentally realize quantum error correction, as it requires multiple qubits and quantum gates with high fidelity. Here we propose a simple quantum error-correcting code for the detected amplitude damping channel. The code requires only two qubits. We implement the encoding, the channel, and the recovery on an optical platform, the IBM Q System, and a nuclear magnetic resonance system. For all of these systems, the error correction advantage appears when the damping rate exceeds some threshold. We compare the features of these quantum information processing systems used and demonstrate the advantage of quantum error correction on current quantum computing platforms.

© 2020 Science China Press. Published by Elsevier B.V. and Science China Press. All rights reserved.

1. Introduction

Quantum computing, as the next generation of information technology, exploits the superposition principle and quantum entanglement to solve some difficult problems more efficiently than classical computing devices. It is widely believed that quantum computing has potential to realize an exponential advantage for certain problems, such as prime factor decomposition [1] and principal component analysis [2], over current classical algorithms. In addition, some pioneering work also connects quantum computing with other research fields, including quantum simulation, cryptography, and machine learning. Since the concept of quantum computers came into being, several quantum systems, such as linear optical systems, nuclear magnetic resonance (NMR) systems, trapped ion systems, and superconducting circuits, were regarded as possible platforms to implement quantum computers [3]. Over

the past decade, hardware for quantum computers has undergone an astonishing evolution, especially on superconducting circuits and trapped ion systems. Very recently, Google announced that they had achieved quantum advantage using a programmable superconducting processor with 53 qubits [4]. In the field of trapped ions, IonQ also made a presentation about their quantum computer with 79 processing qubits [5]. On the other hand, IBM and Rigetti released their online quantum platforms linking with real superconducting quantum computers to the public. We are now entering a new era in quantum technology, namely the Noisy Intermediate-Scale Quantum (NISQ) [6] era, even with fault-tolerant quantum computing still a distant dream.

Theoretically, quantum computers could outperform classical computers dramatically. However, it still presents a major obstacle that the information encoded on qubits is very vulnerable to the noise induced by inevitable interaction between the qubits and the environment. Almost all the proposed physical implementations encounter quantum errors, including decoherence, imperfect quantum logic gates, and readout error. A direct approach to reduce quantum errors is improving the quantum computers on the physical level. At present, in superconducting quantum proces-

 $^{* \ \} Corresponding \ authors.$

E-mail addresses: gyxiang@ustc.edu.cn (G.-Y. Xiang), xint@sustech.edu.cn (T. Xin), zengb@ust.hk (B. Zeng).

¹ These authors contributed equally to this work.

sors, single-qubit and two-qubit gate fidelities exceed 99.9% and 99.5% [4], respectively. Benefiting from well-developed quantum control techniques, such as composite pulses [7], refocusing pulses [8], and the Gradient Ascent Pulse Engineering (GRAPE) algorithm [9], fidelities of quantum gates can reach even higher accuracy on NMR quantum computers.

While improving the quantum hardware is in the main focus of research right now, it is impossible to completely eliminate the errors in quantum computers. To realize a reliable quantum computer, additional techniques are required. Quantum error correction (QEC) [10-12], protecting quantum information against unwanted operations, has spawned considerable interest from both physicists and mathematicians. Some initial theoretical results in this field focused on quantum error-correcting codes (OECCs) [13–17], other approaches are noiseless quantum codes and decoherence free subspaces [18]. The discovery of OECCs enhanced the possibility of building a quantum computer and has further led to the concept of fault-tolerant quantum computation [17,19,20]. One important QECC is the surface code with a fault tolerance threshold of 1×10^{-2} for each error source [21,22]. Previous experimental progress for some quantum errorcorrecting codes demonstrated the power of QECC for several qubits for linear optics [23], trapped ions [24,25], NMR [26], and superconducting circuits [27-30]. Measurement-based feedback [30,31] and other advanced techniques have also been developed to implement error correction, in order to build a continuoustime and automatic quantum error correction system.

In this paper, we report on the implementation of a channel-adapted detected amplitude quantum code using a two-qubit system on various platforms: a quantum optical system, the IBM Q Experience superconducting circuit, and an NMR quantum system. The experiments on different quantum systems successfully demonstrate the power of the error-correcting code with observable improvement of the fidelity when the damping rate is larger than a threshold γ_c .

2. Model

In a typical quantum information process, like the one shown in Fig. 1, quantum information might be subject to spontaneous decay with detected photon emission, which is modelled by the dectected amplitude channel. Generally, a dectected amplitude damping channel is composed of an amplitude damping channel (denoted by Φ_{AD} , see the Supplementary materials) and an ancilla system indicating whether damping has occurred. The channel can be described by Kraus operators with an extra qubit,

$$\Phi_{\rm DJ}(\rho) = \sum_{i} \left(A_i \rho A_i^{\dagger} \right) \otimes |i\rangle \langle i|_{\rm anc}, \tag{1}$$

where $A_0 = \begin{pmatrix} 1 & 0 \\ 0 & \sqrt{1-\gamma} \end{pmatrix}$ and $A_1 = \begin{pmatrix} 0 & \sqrt{\gamma} \\ 0 & 0 \end{pmatrix}$. The construction of quantum error-correcting codes for the detected amplitude channel has been discussed in Refs. [32–34]. The simplest code correcting a single error of the detected amplitude channel needs only two qubits, and hence can be implemented on a present quantum computer. Based on the analysis in Ref. [32], we firstly encode the initial state $|\psi\rangle=\alpha|0\rangle+\beta|1\rangle$ onto the basis $|+\rangle|+\rangle$ and $|-\rangle|-\rangle$ using a controlled-NOT (CNOT) gate followed by two Hadamard gates,

$$\alpha|0\rangle + \beta|1\rangle \rightarrow \alpha|+\rangle|+\rangle + \beta|-\rangle|-\rangle.$$
 (2)

For the two-qubit code given by Eq. (2), there are two standard error correction protocols derived from the parity-check code [35], denoted by Standard A and B. Additionally, using the polar decomposition method in the Supplementary materials, we obtain Optimal Recovery which will lead a higher fidelity. The optimal

recovery operation will depend on the damping parameter γ , meaning it is a "channel-adaptive" error correction scheme, and its optimality was proved in Ref. [36].

For the two-qubit code given by Eq. (2), Standard Correction A/B protocols can be derived as follows:

- (1) If A_0A_1 (or A_1A_0) happens, discard the qubit on which A_1 happened. On the other qubit, apply X to compensate for the phase error introduced by A_1 acting differently on $|+\rangle$ and $|-\rangle$.
- (2) If A_0A_0 happens, directly decode the two qubits.
- (3) If A_1A_1 happens, the quantum state $|\psi\rangle$ is converted to the state $|00\rangle$. To maximize the fidelity, we transform it to an equally weighted superposition state $\frac{1}{\sqrt{2}}(|0\rangle+|1\rangle)$. There are two different schemes to create an equally weighted superposition state which we refer to as Standard Correction A/B (see Table S2 online), respectively.

The Optimal Recovery operators are derived in the Supplementary materials. We find a pair of recovery operations V_3 and V_4 that can be implemented by Pauli gates, the Hadamard gate, a CNOT gate and general single-qubit three-parameter rotation gates. The two recovery operations have the form $V_3 = U_1^\dagger H$ and $V_4 = H U_2^\dagger X$, where

$$U_1 = \frac{1}{\sqrt{(1+t)^2 + (1-s)^2}} \begin{pmatrix} -t - 1 & s - 1 \\ -s + 1 & -t - 1 \end{pmatrix},\tag{3}$$

$$U_2 = \frac{1}{\sqrt{(1+t)^2 + (1-s)^2}} \begin{pmatrix} -s+1 & t+1\\ -t+1 & -s+1 \end{pmatrix},\tag{4}$$

where the parameters s and t are given by

$$s = \frac{\sqrt{2}}{\sqrt{1 + (1 - \gamma)^2}}$$
 and $t = \frac{\sqrt{2}(1 - \gamma)}{\sqrt{1 + (1 - \gamma)^2}}$. (5)

The general setup of the circuit for both Standard Correction A/B and Optimal Recovery is shown in Fig. 1. Information on the specific circuits is given in Table S1 (online) and Fig. 3.

3. Scheme and results

Photons as a kind of "flying qubits" are widely used for quantum information processing and simulation. In a linear optics system, single qubit operations can be implemented with high fidelity as photons are essentially decoherence-free and are not affected by the environment. However, two-qubit gates, like the CNOT gate, become a challenge as it is difficult to let photons interact. We are using optical qubits encoded in the polarization degree of freedom to demonstrate quantum error correction.

In 2018, IBM Q released a 14-qubit transmon superconducting quantum processor (Fig. 2b), IBM Q 16 Melbourne, which is accessible via Qiskit, an open-source framework for quantum computing on IBM Q Experience. The average fidelity of single qubit operations exceeds 99.0%, and the fidelity of the CNOT operation is nearly 82.7% to 95.2%. The pulse durations are 100 and 348 ns for single qubit rotation gates and CNOT gates based on the cross-resonance interaction, respectively. In addition, two-qubit gates are only permitted between neighboring qubits that are connected by a superconducting bus resonator (see the inset in Fig. 2b). More information on the qubits and quantum gates on *IBM Q 16 Melbourne*, such as the dephasing times and gate fidelities, can be found on the IBM Q site https://quantumexperience.ng.bluemix.net/qx/devices.

NMR quantum computing is one of the first proposed schemes for building a quantum computer with spin-1/2 nuclei, such as ¹H

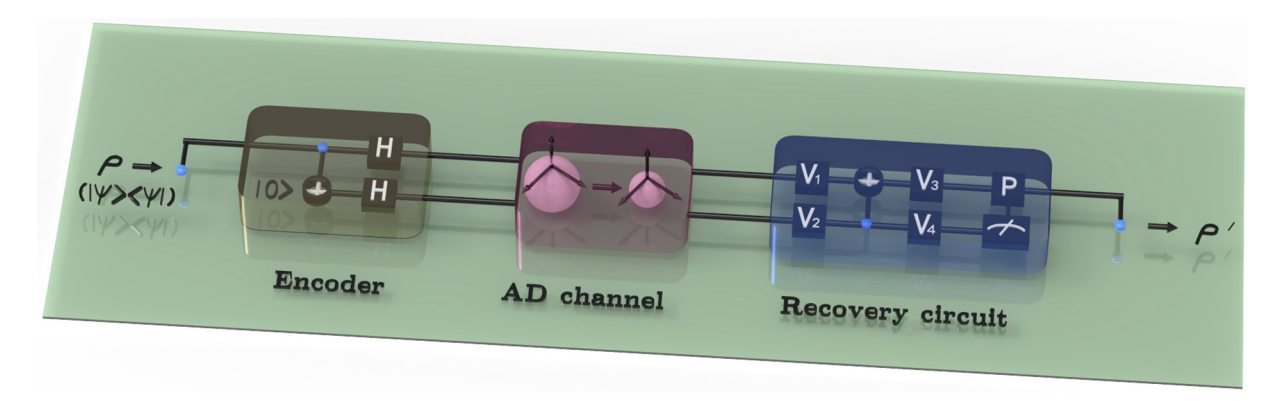


Fig. 1. (Color online) The model of the quantum communication system with an amplitude damping channel. The encoder maps an arbitrary initial single-qubit state $\rho = |\psi\rangle\langle\psi|$ to the code space using two qubits. Then a detected amplitude damping channel acts on each of the two qubits. Finally we apply the recovery circuit (including decoding), which discards the second qubit, obtaining a single-qubit output state $\rho\prime$ that ideally has a large overlap with the input state $|\psi\rangle$.

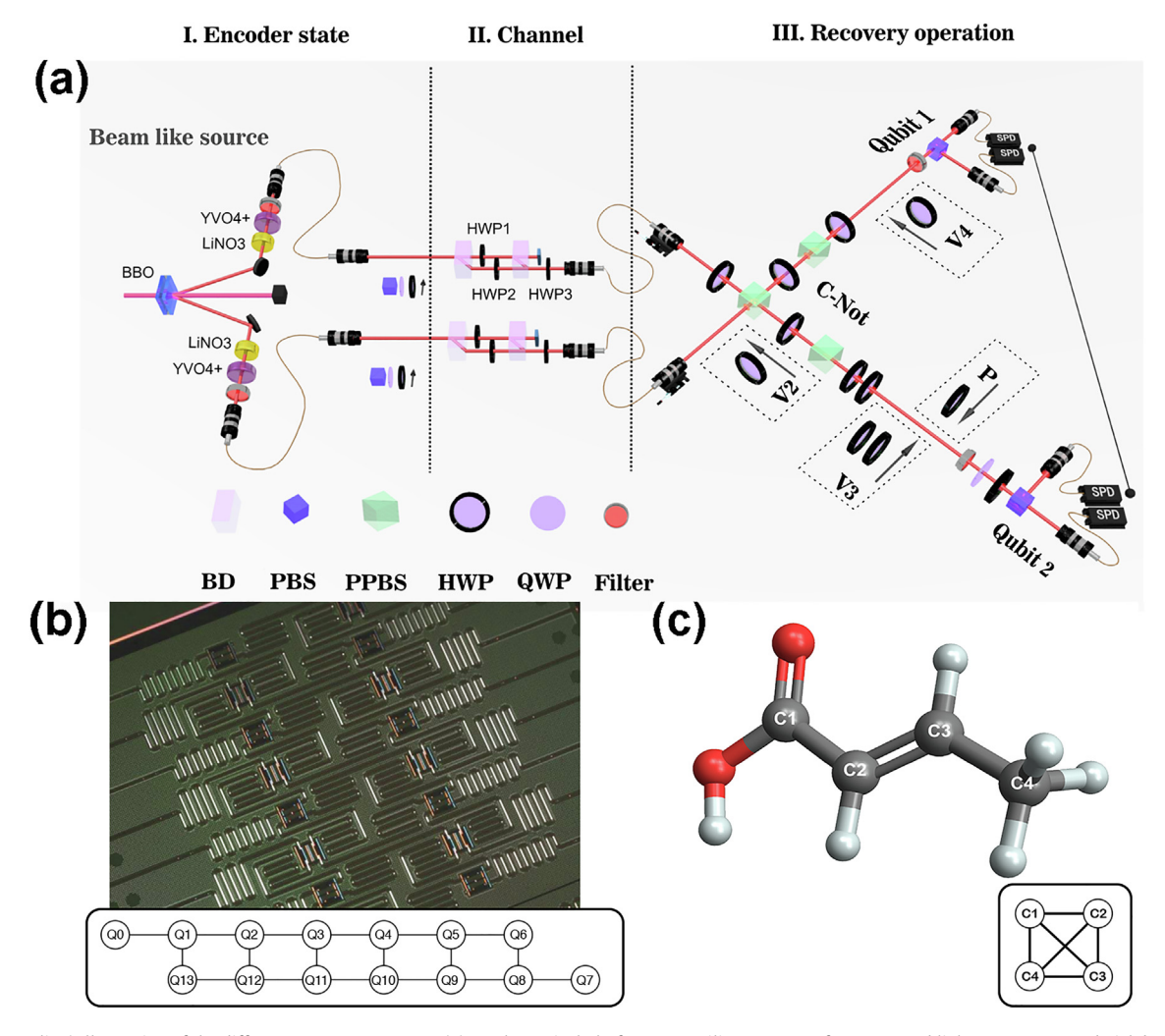


Fig. 2. (Color online) Illustration of the different quantum systems. (a) On the optical platform, we utilize a 390 nm femto-second light to pump a sandwich beamlike phase-matching β -barium-borate (BBO) crystal to generate pairs of polarization entangled photon as qubits. (b) IBM Q 16 Melbourne, consisting of 14 superconducting qubits connected via microwave resonators, together with the coupling structure (the photo of quantum processor comes from "IBM Q 16 Melbourne backend specification V1". Retrieved from https://quantum-computing.ibm.com). (c) The four qubits on the Crotonic acid are given by the spin-1/2 nuclear spins of ¹³C. Each of the four spins couples to the other three.

or ¹³C. With a time-varying radio frequency (RF) field and the free evolution between the different spins, arbitrary unitary transforms can be implemented in the NMR quantum computer. In our exper-

iment, we used a Crotonic acid specimen. The four qubits on the Crotonic acid are represented by the spin-1/2 ¹³C nuclear spins, labeled as C_1 to C_4 as shown in Fig. 2c. The decoherence times of

the Crotonic acid are $T_1 \approx 1500$ ms and $T_2^* \approx 550$ ms. All NMR experiments were carried out on a Bruker DRX 600 MHZ spectrometer at room temperature.

For the three quantum systems, quantum optical platform, IBM Q superconducting circuit and NMR system (see the Supplementary materials), we have implemented different variants of quantum error-correction for the detected amplitude damping channel. In this model of decoherence, an excited state decays to the ground state with some probability. Monitoring the system, one obtains the additional classical information whether the system has decayed or not. Owing to the features of the different systems, we first adapt our scheme to the particular device and decompose the quantum circuits into basic gates native for each system. In Fig. 3, we give the quantum circuits that we employed in the realistic experimental process.

As shown in Fig. 2a, a 390 nm femto-second light (frequency-doubled from a 780 nm mode-lock Ti:sapphire pulsed laser with a pulse width of 150 fs and repetition rate 76 MHz) pumps a sand-wich beamlike phase-matching β -barium-borate (BBO) crystal to generate pairs of polarization entangled photon $\frac{1}{\sqrt{2}}(|HV\rangle + |VH\rangle)$ in the spontaneous parametric down-conversion (SPDC) process. Based on the entangled photons source, whose fidelity is 0.9917 \pm 0.006, we can prepare the desired encoded state for the six different states (see the Supplementary materials) by using polarization beam splitters (PBS), half wave plates (HWP), and quarter wave plates (QWP). The detailed configurations are given in Table S2 (online).

As illustrated in the middle part of Fig. 2a, for the optical platform we use an interferometer to implement the detected amplitude damping channel [37]. Here two beams displacers are used to construct an interferometer [38,39]. For the operator A_0 , the amount of damping γ is adjusted by rotating HWP1 placed between two BDs by the angle θ , with $\sin^2 2\theta = 1 - \gamma$. And, regarding A_1 , the rotated angle of HWP1 and γ has a relation $\gamma = \sin^2 2\theta$.

The two interferometers together (middle part of Fig. 2a) simulate the four error pattern: A_0A_0 , A_0A_1 , A_1A_0 , and A_1A_1 . In the error correction part, we use the method of Refs. [40–42] to implement an all-optical CNOT gate, which is constructed by partially polarizing beam splitters (PPBS) and HWPs. To quantify the quality of the CNOT gate, we perform quantum process tomography showing that the fidelity between the implemented and the ideal gate is about 88.5% [43]. The errors are mainly caused by the mode mismatch of the Hong-Ou-Mandel (HOM) interferometer. In our experiment, the error patterns and the corresponding recovery operations are given in Table S1 (online), where the gates H and X can be easily realized by rotating the HWP by 22.5° and 45° respectively. The detailed information about the damping channel, the CNOT gate, and the case without error correction are given in the Supplementary materials.

On IBM O and the NMR system we use two ancilla gubits to implement the two-qubit detected amplitude channel. The qubits of IBM Q 16 Melbourne and the Crotonic acid (see Fig. 2b and c) meet the required coupling structure (other quantum chips from IBM Q do not match this connectivity map). To be more concrete, Q_5, Q_6, Q_8, Q_9 on IBM Q 16 Melbourne are selected because the average error rates of CNOTs between those qubits are lower than others (Q_5, Q_6) are used for the encode qubits and Q_8, Q_9 are for ancillas). On the NMR system, we select C_2, C_3 for the encode qubits and C_1, C_4 for ancillas. Generally, there are three parts in the quantum circuit, encoder, amplitude channel, and recovery circuit (containing the decoder) in the IBM Q and the NMR experiments, as shown in Fig. 3b. First, we prepare the initial state $|\psi\rangle$ by a single qubit rotation of Q₅. A CNOT gate and two Hadamard gates compose the encoder. With controlled-y-rotation gates $R_{v}(\theta)$ acting on the ancillas and CNOT gates acting on the encoded qubits, we can simulate the two-qubit detected amplitude channel [12]. The relation between the damping ratio γ and the rotation angle θ is $\gamma = \sin^2(\theta/2)$. Measuring the ancilla qubits reveals which type of error occurred. If the result is $|0\rangle$, A_0 has occurred on the

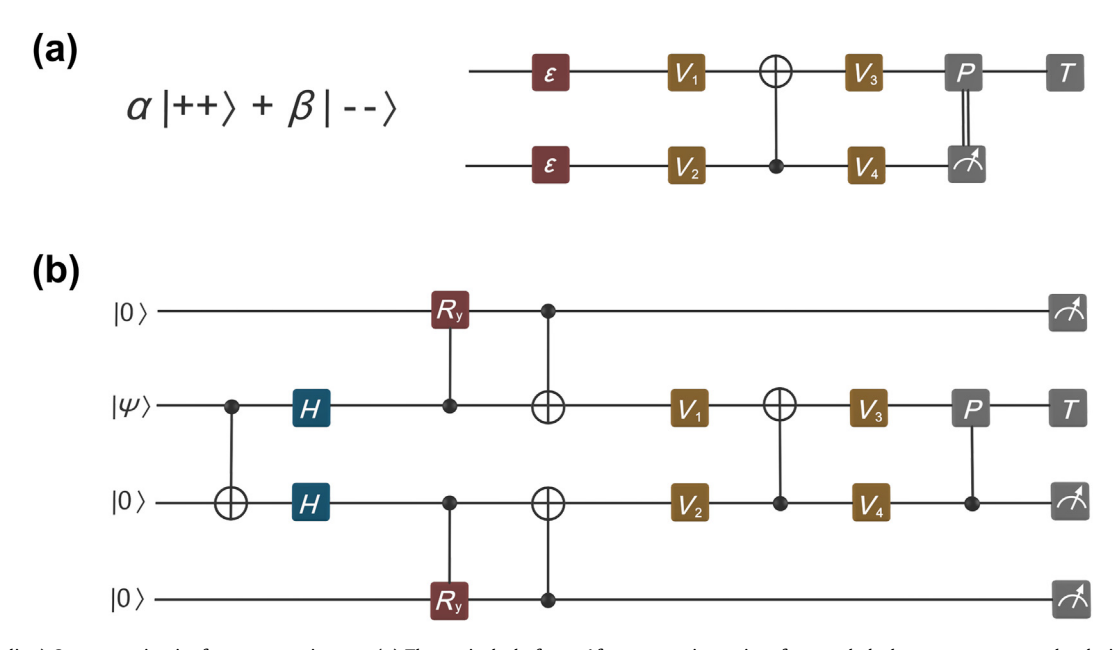


Fig. 3. (Color online) Quantum circuits for our experiments. (a) The optical platform. After generating pairs of entangled photon, we prepare the desired encoded state $\alpha|++\rangle+\beta|--\rangle$ with polarization beam splitters and wave plates, see Table S2 (online). The detected amplitude damping channel is depicted by ε. In the error correction part, we implement Standard Correction A (see the Supplemental materials) using four single qubit rotations and a CNOT based on a HOM interferometer. For the reconstruction of the decoded state, we use post-selection on the other qubits. (b) The circuit for IBM Q and the NMR system. Artificial amplitude damping channels are implemented by a controlled-y-rotation from the encoded qubits to the ancillas and the subsequent CNOT gates. Measuring the ancilla qubits at the end reveals which error has occurred. The single-qubit gates V_1, V_2, V_3 , and V_4 in the recovery circuit depend on the particular error. To simplify the circuit, we run experiments with all settings and use post-selection on the corresponding measurement results of the ancillas. At the end, we use single-qubit state tomography on the second qubit to reconstruct the density matrix.

corrsponding encoded qubit, while A_1 has occurred when the result is $|1\rangle$. Recovery circuits optimized for IBM Q 16 Melbourne and the NMR system are shown in Fig. 3b. To extract the quantum density matrix of the decoded qubit, we use quantum state tomography (QST) and post selection (see the Supplementary materials), measuring the output of the same quantum circuit in different bases. For the IBM Q experiments, we construct the circuit with three-parameter single qubit rotation gates $U_3(\theta,\lambda,\phi)$ and CNOT gates. For the NMR experiments, we generate the pulse sequences of the encoder, two-qubit amplitude damping channel, and recovery circuit using an optimized shape pulse sequence with a total time of 61 ms.

The main experimental results for the three systems are shown in Fig. 4. The fidelity of the effective communication channel is plotted as a function of the damping parameter γ . For the three different systems, we show the effective regions for which Optimal Recovery respectively (Standard Correction A for the optical platform) yields a higher fidelity than using no error correction. Without error correction, the optical platform shows a great advantage in comparison to the other two systems, with the performance of IBM Q being the lowest. However, with error correction, the situation changes dramatically. For the optical platform, the state fidelity drops already a lot at $\gamma = 0$, while adding error-correcting only slightly reduces the fidelity at $\gamma = 0$ for IBM Q. Exhibiting the largest effective region (lighter blue), our error correction scheme exhibits a good performance on the NMR system, and the maximal improvement at $\gamma \approx 0.6$ reaches approximately 0.2. For IBM Q, the improvement (red region) is smaller, but it is still given for a large range of damping parameters γ . For the optical platform, error correction improves the overall fidelity only a little for $\gamma > 0.83$.

On the optical platform (see Fig. S4 online) we perform experiments with Standard Correction A and without correction. At the

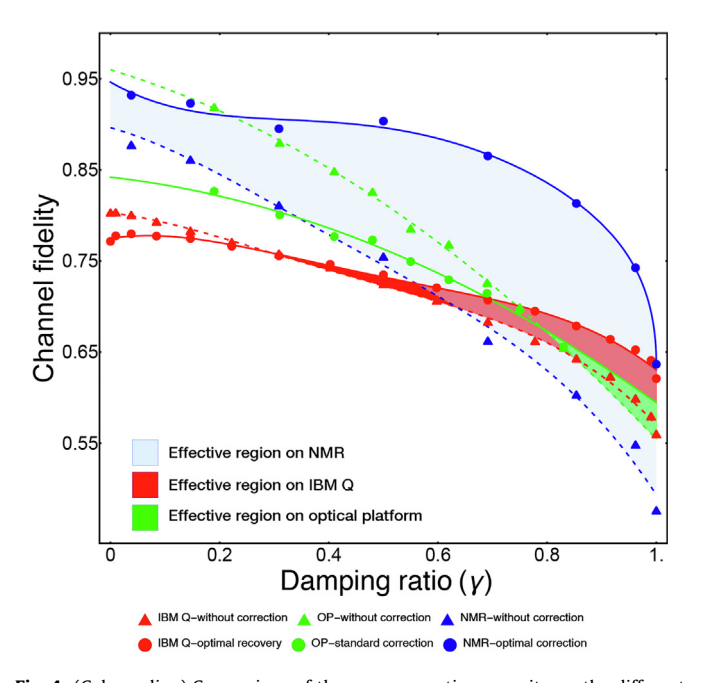


Fig. 4. (Color online) Comparison of the error correction capacity on the different systems. The red, green, and blue regions characterize the effective region enclosed by the fidelity curves for IBM Q, the optical platform (OP), and the NMR system, respectively. The solid and dashed lines are polynomial fits to our experimental data. The solid lines represent Optimal Recovery, and the dashed lines correspond to the case "without corrections". For IBM Q and the optical platform, when the damping ratio γ is small, Optimal Recovery (Standard Correction A) performs worse initially because of the limited fidelity of the additional encoding operations. When the damping ratio γ increases, Optimal Recovery reveals its capacity gradually. Average error bars are about 1.1% for IBM Q [44], 0.4% and 0.7% for the optical platform and NMR system (see Figs. S4a, S5a, and S6a online).

mercy of the bad fidelity of implementing the CNOT by HOM interference, we find that at lower damping probabilities ($\gamma=0.17-0.83$), the fidelity for the state without correction is larger than with standard correction. However, if the damping probability γ is larger than 0.83, standard error correction will be better. This demonstrates some limited improvement using quantum error correction.

Fig. S5 (online) shows the result for IBM Q averaging 4096 runs for 16 sample points. For $\gamma \in [0.0,0.36)$, no correction yields a higher fidelity than Optimal Recovery since "without correction" involves only two qubits. Generally, it is ubiquitous to QEC that the encoded states get worse initially as the encoding operations reduce the fidelity. The blue star plotted at $\gamma=0.36$ in Fig. S5a (online) indicates the intersection when the overall fidelity of "Optimal Recovery" equals "without correction". When the damping parameter γ increases, both Standard Correction A and Standard Correction B show the capacity of error correction, but neither outperforms Optimal Recovery.

The results for the NMR system are show in Fig. S6 (online). Optimal Recovery, Standard Correction A, as well as Standard Correction B show substantial improvements in comparison to "without correction", indicating the power of quantum error correction. Furthermore, the state fidelity curves for Standard Correction A and Standard Correction B exhibit faster decay than the curve for Optimal Recovery, revealing that Optimal Recovery is indeed the best error correction scheme for the detected amplitude damping channel, which matches the theoretical results.

4. Discussion and conclusion

The experiments mainly demonstrate the potential to realize quantum error correction on a quantum computer in the NISQ era by implementing an optimal error-correcting code for detected amplitude damping on IBM Q, an optical platform, and an NMR system. All experiments provide evidence that the advantage of quantum error correction can even be revealed on a present quantum computer, with only a few qubits and faulty quantum gates. For all three systems, Optimal Recovery shows eventually an improvement in comparison to "without correction". On the other hand, for small damping parameters γ , the correction scheme does not come into effect on the optical platform and on IBM Q.

Our experiments also reveal the underlying relation between the ability of quantum control and the performance of quantum error correction. In a typical quantum information process, quantum errors mainly stem from imprecise readout, decoherence, and faulty CNOT gates.

Firstly, we consider the influence of imprecise readout. The readout error for the optical platform and the NMR system can be neglected because for these systems, the precision of readout is close to 99.9%. On the IBM Q platform, however, the average error rate of readout is nearly 5.0%, see Table S3 (online). Apparently, the readout error only contributes a fraction of the entire infidelity in our experiments.

The qubit quality, especially the coherence time, is also an important factor for the performance of the quantum error-correcting code. A rough estimate for the state $\frac{1}{\sqrt{2}}(|0\rangle+|1\rangle)$ shows that the decoherence error contribution from T_2 for IBM Q and the NMR system are 3.5% and 9.9%, respectively (see the Supplementary materials). Therefore, the decoherence is not the main source of the infidelity in IBM Q experiments, but may cause the dominant error in the NMR system.

For the optical system, substantial infidelity is contributed by the CNOT based on HOM interference. When adding the CNOT to the recovery circuit, the total shot numbers of photons will be suppressed by the PPBS crystal. We denote the phenomenon by shot

loss. If we use ideal probabilities that the errors happen instead of the real probabilities in the experiments to reconstruct the effective density matrix, the correcting effect will enhance, see Fig. S6 (online). A similar effect occurs for IBM Q because of crossresonance CNOT gates. This phenomenon stems from ZZ-crosstalk in the superconducting qubit chips [45]. To reconstruct the density matrix with ideal probabilties, even Standard Correction A shows the capcity to improve the channel fidelity in Fig. S6 (online). However, in the NMR experiments, we use the GRAPE algorithm to generate the total pulse sequence with a precision of 99.9%, which gives a great improvement to CNOTs and other operations.

In conclusion, our experiments demonstrate that the quality of CNOT mainly influences the performance of quantum error correction. CNOT operations, at the core of both encoder and decoder, play a unique role to generate entanglement in both quantum error correction and quantum computing. Our results motivate further investigations to improve the precision of CNOT operations and indicate the route towards viable quantum error correction in the NISQ era.

Conflict of interest

The authors declare that they have no conflict of interest.

Acknowledgments

We thank Dawei Lu, Shuming Cheng, Kevin Resch, Runyao Duan for fruitful discussions. We gratefully acknowledge use of the IBM Q for this work. The views expressed are those of the authors and do not reflect the official policy or position of IBM or the IBM Q team. Yuan-Yuan Zhao is supported by the National Natural Science Foundation for the Youth of China (11804410). Markus Grassl acknowledges partial support by the Foundation for Polish Science (IRAP project, ICTQT, contract No. 2018/MAB/5, cofinanced by EU within the Smart Growth Operational Programme). Guo-Yong Xiang is supported by the National Natural Science Foundation of China (11574291, 11774334). Tao Xin and Xinfang Nie are supported by the National Natural Science Foundation of China (11975117, 11875159, 11905099, and U1801661), Guangand Applied Basic Research (2019A1515011383), and Guangdong Provincial Key Laboratory (2019B121203002). Zhang-Qi Yin is supported by National Natural Science Foundation of China (61771278) and Beijing Institute of Technology Research Fund Program for Young Scholars.

Author contributions

Markus Grassl and Bei Zeng designed the study. Qihao Guo performed the IBM Q experiment under the supervision of Zhang-Qi Yin. Yuan-Yuan Zhao conducted the optical experiment. Qihao Guo and Xinfang Nie performed the NMR experiment. Tao Xin provided support about NMR system. Guo-Yong Xiang, Zhang-Qi Yin and Bei Zeng supervised the project. Qihao Guo, Yuan-Yuan Zhao, Markus Grassl, Zhang-Qi Yin and Bei Zeng wrote the manuscript with feedback from all authors. Qihao Guo and Yuan-Yuan Zhao contributed equally to this work.

Appendix A. Supplementary materials

Supplementary materials to this article can be found online at https://doi.org/10.1016/j.scib.2020.07.033.

References

- [1] Shor PW. Algorithms for quantum computation: discrete logarithms and factoring. In FOCS, 124–134, IEEE; 1994..
- [2] Lloyd S, Mohseni M, Rebentrost P. Quantum principal component analysis. Nat Phys 2014;10:631.
- [3] Ladd TD, Jelezko F, Laflamme R, et al. Quantum computers. Nature 2010;464:45.
- [4] Arute F, Arya K, Babbush R, et al. Quantum supremacy using a programmable superconducting processor. Nature 2019;574:505–10.
- [5] Wright K, Beck KM, Debnath S, et al. Benchmarking an 11-qubit quantum computer. Nat Commun 2019:10:5464.
- [6] Preskill J. Quantum computing in the NISQ era and beyond. arXiv:1801.00862, 2018
- [7] Levitt MH. Composite pulses. Prog Nucl Magn Reson Spectrosc 1986:18:61–122.
- [8] Bendall MR, Gordon RE. Depth and refocusing pulses designed for multipulse NMR with surface coils. | Magn Reson 1983;53:365–85.
- [9] Rowland B, Jones JA. Implementing quantum logic gates with gradient ascent pulse engineering: principles and practicalities. Philos 2012;370:4636–50.
- [10] Calderbank AR, Shor PW. Good quantum error-correcting codes exist. Phys Rev A 1996;54:1098.
- [11] Gottesman D. An introduction to quantum error correction. PSAM 2002:58:221–36.
- [12] Nielsen MA, Chuang IL. Quantum Comp and Quantum Inf. 10th ed. New York, NY, USA: Cambridge University Press; 2011.
- [13] Leung DW, Nielsen MA, Chuang IL, et al. Approximate quantum error correction can lead to better codes. Phys Rev A 1997;56:2567.
- [14] Chao R, Reichardt BW. Quantum error correction with only two extra qubits. Phys Rev Lett 2018;121:050502.
- [15] Grassl M, Kong L, Wei Z, et al. Quantum error-correcting codes for qudit amplitude damping. IEEE Trans Inf Theory 2018;64:4674–85.
- [16] Beale SJ, Wallman JJ, Gutiérrez, et al. Quantum error correction decoheres noise, Phys Rev Lett 2018;121:190501.
- [17] DiVincenzo DP, Shor PW. Fault-tolerant error correction with efficient quantum codes. Phys Rev Lett 1996;77:3260.
- [18] Lidar DA, Bacon D, Whaley KB. Concatenating decoherence-free subspaces
- with quantum error correcting codes. Phys Rev Lett 1999;82:4556–9.
 [19] DiVincenzo DP. The physical implementation of quantum computation.
- Fortschritte der Phys 2000;48:771–83. [20] Steane AM. Overhead and noise threshold of fault-tolerant quantum error correction. Phys Rev A 2003;68:042322.
- [21] Wang DS, Fowler AG, Hollenberg LC. Surface code quantum computing with error rates over 1%. Phys Rev A 2011;83:020302.
- [22] Barends R, Kelly J, Megrant A. et al. Logic gates at the surface code threshold: Superconducting qubits poised for fault-tolerant quantum computing. arXiv:1402.4848, 2014..
- [23] Braunstein SL. Quantum error correction for communication with linear optics. Nature 1998;394:47.
- [24] Zhang S, Lu Y, Zhang K. et al. Error-mitigated quantum gates exceeding physical fidelities in a trapped-ion system. arXiv:1905.10135, 2019.
- [25] Schindler P, Barreiro JT, Monz T, et al. Experimental repetitive quantum error correction. Science 2011;332:1059–61.
- [26] Cory DG, Price M, Maas W, et al. Experimental quantum error correction. Phys Rev Lett 1998;81:2152.
- [27] Ofek N, Petrenko A, Heeres R, et al. Extending the lifetime of a quantum bit with error correction in superconducting circuits. Nature 2016;536:441.
- [28] Reed MD, DiCarlo L, Nigg SE, et al. Realization of three-qubit quantum error correction with superconducting circuits. Nature 2012;482:382.
- correction with superconducting circuits. Nature 2012;482:382.
 [29] Rosenblum S, Reinhold P, Mirrahimi M, et al. Fault-tolerant detection of a
- quantum error. Science 2018;361:266–70.
 [30] Hu L, Ma Y, Cai W, et al. Quantum error correction and universal gate set operation on a binomial bosonic logical qubit. Nat Phys 2019;15:503.
- [31] Cardona G, Sarlette A, Rouchon P. Continuous-time quantum error correction with noise-assisted quantum feedback. arXiv:1902.00115, 2019..
- [32] Grassl M, Ji Z, Wei Z, et al. Quantum-capacity-approaching codes for the detected-jump channel. Phys Rev A 2010;82:062324.
- [33] Alber G, Beth T, Charnes C, et al. Stabilizing distinguishable qubits against spontaneous decay by detected-jump correcting quantum codes. Phys Rev Lett 2001;86:4402.
- [34] Alber G, Beth T, Charnes C, et al. Detected-jump-error-correcting quantum codes, quantum error designs, and quantum computation. Phys Rev A 2003;68:012316.
- [35] Grami A. Chapter 10 error-control coding. In: Grami A, editor. Introduction to Digital Communications. Boston: Academic Press; 2016. p. 409–55.
- [36] Gregoratti M, Werner RF. Quantum lost and found. | Mod Opt 2003;50:915–33.
- [37] Fisher KA, Prevedel R, Kaltenbaek R, et al. Optimal linear optical implementation of a single-qubit damping channel. New J Phys 2012;14:033016.
- [38] Zhao Y-Y, Kurzyński P, Xiang G-Y, et al. Heisenberg's error-disturbance relations: a joint measurement-based experimental test. Phys Rev A 2017;95:040101.
- [39] Zhao Y-Y, Grassl M, Zeng B, et al. Experimental detection of entanglement polytopes via local filters. Npj Quantum Inf 2017;3:11.

[40] Kiesel N, Schmid C, Weber U, et al. Linear optics controlled-phase gate made simple. Phys Rev Lett 2005;95:210505.

- [41] Okamoto R, Hofmann HF, Takeuchi S, et al. Demonstration of an optical quantum controlled-NOT gate without path interference. Phys Rev Lett 2005:95:210506.
- [42] Wu K-D, Hou Z, Zhao Y-Y, et al. Experimental cyclic interconversion between coherence and quantum correlations. Phys Rev Lett 2018;121:050401.
- [43] Ježek M, Fiurášek J, Hradil Z. Quantum inference of states and processes. Phys Rev A 2003;68:012305.
- [44] García-Pérez G, Rossi MAC, Maniscalco S. IBM Q experience as a versatile experimental testbed for simulating open quantum systems. Npj Quantum Inf 2020;6:1–10.
- [45] Harper R, Flammia ST. Fault-tolerant logical gates in the IBM Quantum Experience. Phys Rev Lett 2019;122:080504.



Guo-Yong Xiang received a B.E. degree in Physics Education from Anhui Normal University in 2000 and a Ph.D. degree in Optics from University of Science and Technology of China (USTC) in 2005 respectively. Currently, he is a professor at USTC. He was a research fellow at Griffith University, Australia from 2007 to 2010. His research interest includes quantum optics and quantum information, especially quantum precision measurement and quantum control.



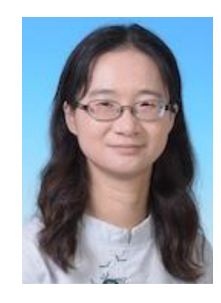
Qihao Guo is currently a research assistant at Southern University of Science and Technology. He received his B.S. degree (Hons) from Xi'an Jiaotong University in 2020. His current research interest includes quantum orbital control, quantum simulation and quantum computation.



Tao Xin is currently an assistant researcher at the Institute of Quantum Science and Engineering of Southern University of Science and Technology. He received a Ph.D. degree from the Department of Physics of Tsinghua University in 2018. His main research directions are spin-based systems for quantum information processing, quantum device characterization via tomography, and quantum machine learning based on parameterized quantum circuits.



Yuan-Yuan Zhao received the B.S. degree in Physics from Henan Normal University in 2012 and the Ph.D. degree in Physics from University of Science and Technology of China (USTC) in 2017, respectively. Now, she works as the assistant researcher at the Peng Cheng Laboratory. Her research mainly focuses on quantum information and quantum measurement.



Bei Zeng is a Professor at the Department of Physics, The Hong Kong University of Science and Technology. She received the B.Sc. and M.Sc. degrees from Tsinghua University. In 2009, she received the Ph.D. degree in Physics from Massachusetts Institute of Technology (MIT). She joined University of Guelph in 2010 and promoted to Professor in 2018. Her research strives to bring us closer to the high rate quantum information transmission, and reliable quantum computation with high noise tolerance and low resource requirement.